Chapter

Magnetic Solitons in Optical Lattice

Xing-Dong Zhao

Abstract

In this chapter, we discuss the magnetic solitons achieved in atomic spinor Bose-Einstein condensates (BECs) confined within optical lattice. Spinor BECs at each lattice site behave like spin magnets and can interact with each other through the static magnetic dipole-dipole interaction (MDDI), due to which the magnetic soliton may exist in blue-detuned optical lattice. By imposing an external laser field into the lattice or loading atoms in a red-detuned optical lattice, the light-induced dipole-dipole interaction (LDDI) can produce new magnetic solitons. The long-range couplings induced by the MDDI and ODDI play a dominant role in the spin dynamics in an optical lattice. Compared with spin chain in solid material, the nearest-neighbor approximation, next-nearest-neighbor approximation, and long-range case are discussed, respectively.

Keywords: spinor Bose-Einstein condensates, spin wave, optical lattice, magnetic soliton

1. Introduction

Soliton can be classified into different species, such as matter-wave soliton, magnetic soliton, optical soliton, and so on [1, 2]. The magnetic solitons, which describe the localized magnetization, are very important excitations in the Heisenberg spin chain in solid system in condensed matter [3]. Because of the defect and impurity in solid material, it is difficult to perform experimental observation and manipulation in these systems. In addition, magnetic solitons originate from the Heisenberg-like short-range exchange interaction between electrons in solid state systems, so the theoretical models and treatment are limited to only the approximation of nearest-neighbor interaction, it is disadvantageous to the study of long-range interaction-induced dynamics.

On the other hand, the spinor ultracold atoms in an optical lattice offer a pure and well-controlled platform to study spin dynamics. If the lattice trapping atoms is deep enough, the spinor atoms undergo a ferromagnetic-like phase transition that leads to a macroscopic magnetization of the condensates array; then, the individual sites become independent with each other. Spinor BECs at each lattice site behave like spin magnets and can interact with each other through the static MDDI, which can cause the ferromagnetic phase transition and the spin wave excitation. It is atomic spin chain in optical lattice [4–7]. By tuning the system parameters, magnetic soliton can be produced; however a key difference of the atomic spin chain from solid-state one is that we are facing a completely new spin system in which the

long-range nonlinear interactions play a dominant role. To demonstrate the high controllability, an external laser can be imposed into the lattice and induce light-induced dipole-dipole interaction (LDDI) to produce new magnetic solitons. In fact, the LDDI can be induced by loading the atoms in a red-detuned optical lattice as used in [5]. However, the method used here has good feasibility, and some novel physical phenomena can be observed.

In order to make comparison with the Heisenberg spin chain, we used the nearest-neighbor approximation and the next-nearest-neighbor approximation in our discussion. In addition, the two approximations are effective and reasonable with some appropriate parameters chosen in experiments.

In this chapter, we are going to be seeing how magnetic soliton in atomic spin chain is, which will be theoretically described. We first discuss the formation of atomic spin chain in optical lattice in Section 2. Then we shift our focus to the condition for magnetic soliton in Section 3. Section 4 presents the conclusion and outlook.

2. Atomic spin chain

2.1 Atomic spin chain with magnetic dipole: dipole interaction

The spinor BECs can be trapped within one-, two-, and three-dimensional optical lattices with different experimental techniques; however, we only take one-dimensional case as an example. As depicted in **Figure 1**, the atomic gases with $F = 1$ are trapped in a one-dimensional optical lattice, which is formed by two π-polarized laser beams counter-propagating along the y-axis. The light-induced lattice potential takes the form:

$$V_L(\boldsymbol{r}) = U_L \exp\left(-{r_\perp}^2/{W_L}^2\right) \cos^2(k_L y) \tag{1}$$

where $r_\perp = \sqrt{x^2 + z^2}$, $k_L = 2\pi/\lambda_L$ is the wave number, W_L the width of the lattice beams, and the potential depth $U_L = \hbar|\Omega|^2/6\Delta$ with Ω being the Rabi frequency and Δ being laser detuning.

It has been theoretically and experimentally demonstrated that the condensate trapped in optical lattice undergoes a superfluid-Mott-insulator transition as the depth of the lattice wells is increased. If the lattice potential is deep enough, the condensate is divided into a set of separated small condensates equally located at each lattice site, which forms the atomic chain. The condensate localized in each lattice site is approximately in its electronic ground state, while the two lattice laser beams are detuned far from atomic resonance frequency, and the laser detuning

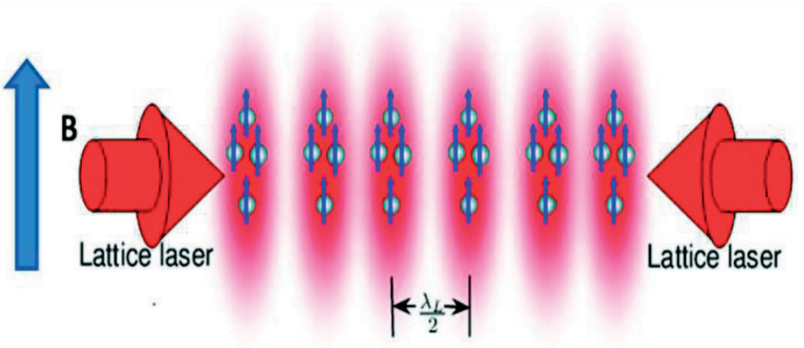

Figure 1.
Schematic diagram of spinor BECs confined in a one-dimensional optical lattice. A strong static magnetic field B is applied to polarize the ground-state spin orientations of the atomic chain along the quantized z-axis.

is defined as $\Delta = \omega_L - \omega_a$, ω_L being laser frequency and ω_a atomic resonant frequency. We classify the optical lattice into two categories: red-detuned optical lattice ($\Delta < 0$) and blue-detuned one $\Delta > 0$. For the former, the condensed atoms are trapped at the standing wave nodes where the laser intensity is approximately zero; the light-induced interactions are neglected in this case. In order to realize ferromagnetic phase transition, a strong static magnetic field $\boldsymbol{B}$ is applied to polarize the ground-state spin orientations of the atomic chain along the quantized z-axis. The Hamiltonian including the long-range MDDI between different lattice sites takes the following form [7–9]:

$$\begin{aligned} H_M = & \sum_m \int d\boldsymbol{r} \left\{ \hat{\psi}_m^\dagger \left(-\frac{\hbar^2}{2M} \nabla^2 + V_L \right) \hat{\psi}_m \right\} \\ & + \sum_{m,\, m',\, n,\, n'} \left\{ \int d\boldsymbol{r} \int d\boldsymbol{r}' \hat{\psi}_m^\dagger \hat{\psi}_{m'}^\dagger \hat{\psi}_{n'} \hat{\psi}_n V_{mm'n'n}^{col}(\boldsymbol{r}, \boldsymbol{r}') \right. \\ & + \frac{1}{2} \int d\boldsymbol{r} \int d\boldsymbol{r}' \hat{\psi}_m^\dagger \hat{\psi}_{m'}^\dagger \hat{\psi}_{n'} \hat{\psi}_n V_1(\boldsymbol{r}, \boldsymbol{r}') \hat{\boldsymbol{F}}_{mn} \cdot \hat{\boldsymbol{F}}_{m'n'} \\ & \left. - \frac{1}{2} \int d\boldsymbol{r} \int d\boldsymbol{r}' \hat{\psi}_m^\dagger \hat{\psi}_{m'}^\dagger \hat{\psi}_{n'} \hat{\psi}_n V_2(\boldsymbol{r}, \boldsymbol{r}') \times \hat{\boldsymbol{F}}_{mn} \cdot (\boldsymbol{r} - \boldsymbol{r}') \hat{\boldsymbol{F}}_{m'n'} \cdot (\boldsymbol{r} - \boldsymbol{r}') \right\} \\ & + \sum_{m,\, n} \int d\boldsymbol{r}\, \hat{\psi}_m^\dagger (-\boldsymbol{\mu} \cdot \boldsymbol{B})_{mn} \hat{\psi}_n \end{aligned} \tag{2}$$

where $\hat{\psi}_m(\boldsymbol{r}, t) (m = \pm 1, 0)$ are the hyperfine ground-state atomic field operators. The total angular momentum operator $\hat{\boldsymbol{F}}$ for the hyperfine spin of an atom has components represented by 3×3 matrices in the $|f = 1, m_f = m\rangle$ subspace. The final term in Eq. (2) represents the effect of polarizing magnetic field, and $\boldsymbol{\mu}$ is magnetic dipole moment. The interaction potential includes the two-body ground-state collisions and the magnetic dipole-dipole interactions, which can be described by the potentials:

$$V_{mm'n'n}^{col}(\boldsymbol{r}, \boldsymbol{r}') = \left[\lambda_s \delta_{m'n'} \delta_{mn} + \lambda_a \hat{\boldsymbol{F}}_{mn} \cdot \hat{\boldsymbol{F}}_{m'n'} \right] \delta(\boldsymbol{r} - \boldsymbol{r}'), \tag{3}$$

$$V_1(\boldsymbol{r}, \boldsymbol{r}') = \frac{\mu_0 {\gamma_B}^2}{4\pi} \frac{1}{|\boldsymbol{r} - \boldsymbol{r}'|^3}, \tag{4}$$

$$V_2(\boldsymbol{r}, \boldsymbol{r}') = \frac{3\mu_0 {\gamma_B}^2}{4\pi} \frac{1}{|\boldsymbol{r} - \boldsymbol{r}'|^5}. \tag{5}$$

In collision interaction potential in Eq. (3), λ_s and λ_a are related to the s-wave scattering length for the spin-dependent interatomic collisions. In the magnetic dipole-dipole interaction potential Eqs. (4) and (5), μ_0 is the vacuum permeability; the parameter $\gamma_B = -\mu_B g_F$ is the gyromagnetic ratio with μ_B being the Bohr magneton and g_F the Landé g factor.

Under tight-binding condition and single-mode approximation, the spatial wave function $\phi_m(\boldsymbol{r})$ of the m-th condensate is then determined by the Gross-Pitaevskii (GP) equation [5]:

$$\left[-\frac{\hbar^2}{2M} \nabla^2 + V_m(\boldsymbol{r}) + \lambda_s (N_m - 1) |\phi_m(\boldsymbol{r})|^2 \right] \phi_m(\boldsymbol{r}) = \mu_m \phi_m(\boldsymbol{r}), \tag{6}$$

with

$$V_m(\boldsymbol{r}) = U_L \exp\left[-{r_L}^2 / W^2 \right] \cos^2(k_L y + m\pi),\ 0 < y < \lambda_L / 2, \tag{7}$$

and N_m is the number of condensed atoms at the m-th site; μ_m is the chemical potential. In this case, the individual condensate confined in each lattice behaves as spin magnets in the presence of external magnetic fields; such spin magnets form a 1D coherent spin chain with an effective Hamiltonian [5, 6]:

$$H_m = \sum_m \left(\lambda_a' \hat{\boldsymbol{S}}_m^2 - \gamma_B \hat{\boldsymbol{S}}_m \cdot \boldsymbol{B} - \sum_{n \neq m} J_{mn}^{mag} \hat{\boldsymbol{S}}_m \hat{\boldsymbol{S}}_n \right), \tag{8}$$

where we have defined collective spin operators $\hat{\boldsymbol{S}}_m$ with components $\hat{S}_m^{\{x,y,z\}}$ and

$$\lambda_a' = \frac{1}{2} \lambda_a \int d\boldsymbol{r} |\phi_m(\boldsymbol{r})|^4. \tag{9}$$

The parameter J_{mn}^{mag} describes the strength of the site-to-site spin coupling induced by the static MDDI. It takes the form:

$$J_{mn}^{mag} = \frac{\mu_0 {\gamma_B}^2}{16\pi\hbar^2} \int d\boldsymbol{r} \int d\boldsymbol{r}' \frac{R_1}{|\boldsymbol{r}'|^5} |\phi_m(\boldsymbol{r})|^2 |\phi_n(\boldsymbol{r} - \boldsymbol{r}')|^2, \tag{10}$$

where μ_0 is the vacuum permeability, $R_1 = |\boldsymbol{r}'|^2 - 3y'^2$. It will be seen from this that the MDDI is determined by many parameters; however, we need to choose a parameter which is easy controllable in the experiment. The realistic interaction strengths of the MDDI and LDDI coupling coefficients have been calculated in ref. [4], in which we find the dependency of the transverse width.

Here, we only consider the ferromagnetic condensates where the spins of atoms at each lattice site align up along the direction of the applied magnetic field (the quantized z-axis) in the ground state of the ferromagnetic spin chain. Because of the Bose-enhancement effect, the spins are very large in these systems. As a result, at low temperature the spins can be treated approximately as classical vectors, and we can replace $\hat{\boldsymbol{S}}_n$ with its average value S_n [1]. From the Hamiltonian (8), we can derive the Heisenberg equation of motion for operator $S_n^{\pm} = S_n^x \pm i S_n^y \left(i^2 = -1\right)$ (normalized by $\hbar$):

$$i \frac{dS_n^+}{dt} = \gamma_B B_z S_n^+ + \sum_{j \neq n} 2 J_{nj}^{mag} \left(S_j^z S_n^+ - S_n^z S_j^+ \right). \tag{11}$$

Equation (11) determines the existence and the propagation of spin waves. From this equation, we can obtain the existence and dynamical evolving of the nonlinear magnetic soliton. In Sec.3, we attempt to show the long-range and controllable characteristics of MDDI and find how this long-range nonlinear dipole-dipole interaction affects the generation of the magnetic soliton. If the static magnetic field $\boldsymbol{B}$ is strong enough, we have:

$$S_n^z = \sqrt{S^2 - S_n^+ S_n^-} = \sqrt{S^2 - S_n^+ S_n^+}. \tag{12}$$

2.2 Atomic spin chain with light-induced dipole-dipole interaction

In fact, the site-to-site interaction can also be tuned by laser field, and the exchange interaction induced by the laser fields also plays an important role in atomic spin chain in optical lattice. We consider that an external modulational laser field is imposed into the system along the $\boldsymbol{y}$-axis. This external laser field is properly

chosen so that a new dipole-dipole interaction will be introduced into the system, i.e., the so-called LDDI. Its Hamiltonian takes the form [10]:

$$H_{opt} = \sum_{m} \sum_{n \neq m} J_{mn}^{opt} \left(\hat{S}_m^- \hat{S}_n^+ + S_m^+ S_n^- \right). \tag{13}$$

Here, the coefficient J_{mn}^{opt} describes the site-to-site spin coupling induced by the LDDI, which has the concrete form:

$$\begin{aligned} J_{mn}^{opt} = & \frac{Q}{144\hbar k_L^3} \int d\boldsymbol{r} \int d\boldsymbol{r}' f_c(\boldsymbol{r}') \exp\left(-\frac{R_2}{W_L^2}\right) \\ & \times \cos(k_L y) \cos[k_L(y - y')] \boldsymbol{e}_{+1} \cdot \boldsymbol{W}(\boldsymbol{r}') \cdot \boldsymbol{e}_{-1} \times |\phi_m(\boldsymbol{r})|^2 |\phi_n(\boldsymbol{r} - \boldsymbol{r}')|^2. \end{aligned} \tag{14}$$

In above integral we define $Q = \gamma |\Omega_1|^2 / \Delta_1^2$ to describe the magnitude of the LDDI; here γ is the spontaneous emission rate of the atoms, and Ω_1 is the Rabi frequency; Δ_1 is the optical detuning for the induced atomic transition. A cutoff function $f_c(\boldsymbol{r}) = \exp(-r/L_c)$ is introduced to describe the effective interaction range of the LDDI, L_c being the coherence length. $R_2 = {r_\perp}^2 + |\boldsymbol{r}_\perp - \boldsymbol{r}_\perp{}'|^2$ with the transverse coordinate $r_\perp = \sqrt{x^2 + z^2}$. The unit vectors have the form:

$$\boldsymbol{e}_0 = \boldsymbol{e}_z, \tag{15}$$

$$\boldsymbol{e}_{\pm 1} = \mp (\boldsymbol{e}_x \pm i \boldsymbol{e}_y), \tag{16}$$

and $\boldsymbol{e}_\alpha (\alpha = x, y, z)$ which are the usual geocentric Cartesian frame. The tensor $\boldsymbol{W}(\boldsymbol{r})$ describes the spatial profile of the LDDI and has the form:

$$\boldsymbol{W}(\boldsymbol{r}) = \frac{3}{4} \left[\left(1 - 3\cos^2\theta\right) \left(\frac{\sin\xi}{\xi^2} + \frac{\cos\xi}{\xi^3} \right) - \sin^2\theta \frac{\cos\xi}{\xi} \right], \tag{17}$$

where we define $\xi = k_L |\boldsymbol{r} - \boldsymbol{r}'|$, and θ is the angle between the dipole moment and the relative coordinate $\boldsymbol{r} - \boldsymbol{r}'$. Being different from MDDI in Eq. (8), it shows that the LDDI in this system leads to the spin coupling only in the transverse direction, i.e., the direction perpendicular to the external magnetic field, as shown in Eq. (13). The total Hamiltonian of the system can be written as [10].

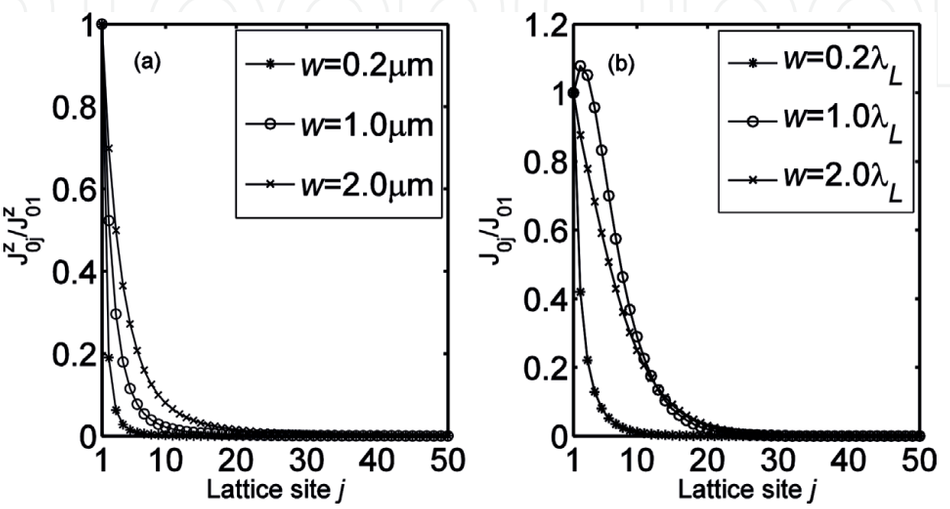

Figure 2.
The spin coupling coefficients $J_{mn}^z = J_{mn}^{mag}$ and J_{ij} as a function of the lattice site index for different transverse widths of the condensate in the MDDI and LDDI dominating optical lattice [4].

$$H = H_m + H_{opt}. \tag{18}$$

Function (11) now has the form:

$$i\frac{d\phi_n}{dt} = \gamma_B B_z \phi_n + \sum_{j=n\pm1} 2SJ_{nj}^{mag}\sqrt{1-\left|\phi_j\right|^2}\phi_n + \sum_{j=n\pm1} 4SJ_{nj}\sqrt{1-|\phi_n|^2}\phi_j. \tag{19}$$

The interaction coefficient J_{ij} satisfies $J_{ij} = J_{ij}^{opt} + \frac{1}{2}J_{ij}^{mag}$.

Figure 2 shows the two spin coupling coefficients varying with the lattice sites and the transverse width of the condensate. It is clear that the spin coupling coefficients are sensitive to the variation of the transverse width W of the condensate and exhibit the similar long-range behavior.

3. Magnetic soliton in atomic spin chain

3.1 Magnetic soliton under the MDDI

To confirm that the magnetic soliton can be formed in this system, we first consider the case that other interactions between spins are absent in this section. Namely if the solitons indeed exist, they can be generated by the MDDI alone $J_{ij} = J_{ij}^{mag}/2$. In the usual way, we set:

$$S_n^{\pm} = S_n^{\pm}/S, \tag{20}$$

$$S_n^{z} = S_n^{z}/S, \tag{21}$$

here S is the magnitude of spin for site n and only depends on the number of atoms trapped in each site. Under the external magnetic field $\boldsymbol{B}$ considered here, we make an assumption that the spin deviation from the quantized z-axis is considerable, which is reasonable when the number of atoms trapped in each site is large; it is achievable according to present experiments. We also assume that the magnitude of the spin deviation s_n will extend over a large number of lattice sites and vary slowly with site index n. Considering the spatial symmetry, we introduce a staggered variable:

$$\phi_n = (-1)^n s_n^+, \tag{22}$$

where ϕ_n is complex; to find the existence conditions of the magnetic soliton modes, we need firstly to get the nonlinear Schrödinger equation (NLSE) for ϕ_n in continuum form, which is expected to be qualitatively correct for solitons in discrete limit.

3.1.1 Nearest-neighbor approximation with the MDDI

Here we firstly consider only the nearest-neighbor (NN) interactions. In other words, we assume that the on-site spin couples only to the spins at its two neighboring sites, and the longer range couplings are artificially cut off. In above equation, for small retortion from the ground state, we have:

$$\sqrt{1-\left|\phi_j\right|^2} \approx 1 - \frac{1}{2}\left|\phi_j\right|^2. \tag{23}$$

Using the slow varying envelope approximation or long-wavelength limit, we have:

$$\left.\frac{d^2\phi(y,t)}{dy^2}\right|_{y=y_n} \approx \frac{\phi_{n+1}+\phi_{n-1}-2\phi_n}{a^2}. \tag{24}$$

where a is the lattice constant. Then we can obtain the continuum limit NLSE for $\phi(y,t)$, namely

$$i\frac{d\phi}{dt} = 2SJ_{01}^{mag}a^2\frac{d^2\phi}{dy^2} + \beta\phi - 4SJ_{01}^{mag}|\phi|^2\phi, \tag{25}$$

where $a = \lambda_L/2$ is the lattice spacing between two adjacent sites, with λ_L being the wave length of the lattice laser beams, and the coefficient $\beta = \gamma_B B_z + 8SJ_{01}^{mag}$. This NLSE is integrable, and it has bright soliton solution if the effects of dispersion and nonlinearity can cancel each other. In other words, the condition for Eq. (25) to have one bright soliton solution is that the coefficient of the second-order spatial derivative term and the coefficient of the cubic nonlinear term are of the same sign [11]. The criterion for the existence of solitons requires:

$$f(W) = -8S^2a^2J_{01}^{mag}2 > 0. \tag{26}$$

Since the spin coupling parameter J_{01}^{mag} is positive, this condition cannot be satisfied, that is to say, there is no one soliton solution in atomic spin chain under the NN approximation. It drives us to in-depth consideration; we should consider more complex interactions, i.e., more site-to-site interactions would be considered.

3.1.2 Next-nearest-neighbor approximation with the MDDI

Even though the long-range effect of the dipole-dipole interaction is obvious, in this section, we consider a case slightly beyond the NN approximation, i.e., the next-nearest-neighbor (NNN) approximation, which is used in some solid-state systems. Under this approximation, each on-site spin is coupled to the four near-neighbor spins, two on its right side and the other two on its left side, respectively. In this case, we set:

$$\alpha_j = J_{0j}^{mag}/J_{01}, \tag{27}$$

$$A_2 = J_{02}/J_{01}, \tag{28}$$

$$\eta = \gamma_B B_z + 4S\left(J_{01}^{mag} + 2J_{01} + J_{02}^{mag} - 2J_{02}\right). \tag{29}$$

Additionally, the second-order spatial derivative is introduced:

$$\left.\frac{d^2\phi(y,t)}{dy^2}\right|_{y=y_n} \approx \frac{\phi_{n+2}+\phi_{n-2}-2\phi_n}{(2a)^2}. \tag{30}$$

Then, we can easily get:

$$\begin{aligned} i\frac{d\phi(y,t)}{dt} &= 4SJ_{01}(1-4A_2)a^2\frac{d^2\phi(y,t)}{dy^2} + \eta\phi(y,t) \\ &\quad - 2SJ_{01}(\alpha_1 + A_2\alpha_2 + 2 - 2A_2)|\phi(y,t)|^2\phi(y,t), \end{aligned} \tag{31}$$

where

$$\eta = \gamma_B B_z + 4S\left(J_{01}^{mag} + 2J_{01} + J_{02}^{mag} - 2J_{02}\right). \tag{32}$$

Because the LDDI is absent in this case, we have:

$$J_{01}^{opt} = 0, \tag{33}$$

$$J_{01} = \frac{1}{2}J_{01}^{mag}, \tag{34}$$

$$\alpha_1 = \alpha_2 = 2. \tag{35}$$

Then, Eq. (31) can be rewritten as [10]:

$$\begin{aligned} i\frac{d\phi(y,t)}{dt} &= 2SJ_{01}^{mag}(1-4A_2)a^2\frac{d^2\phi(y,t)}{dy^2} \\ &\quad + \eta\phi(y,t) - 4SJ_{01}^{mag}|\phi(y,t)|^2\phi(y,t), \end{aligned} \tag{36}$$

where $\eta = \gamma_B B_z + 8SJ_{01}^{mag}$. For two adjacent sites, $A_2 = J_{02}^{mag}/J_{01}^{mag}$ measures the relative strength of the NNN spin coupling to the NN spin coupling. The condition for Eq. (36) to have one soliton solution is

$$f(W) = -8S^2a^2J_{01}^{mag}2(1-4A_2) > 0; \tag{37}$$

we have $A_2 > 0.25$. From the definition of A_2, we can rewrite the condition as $0.25 < A_2 < 1$, which agrees with the instability condition of the extended nonlinear band edge spin wave modes in the linear stability analysis in Ref. [4]. It means that one soliton solution can exist in atomic spin chain after the NNN interactions between spins are considered. To a certain extent, this result is very useful because the NNN approximation is good enough to describe this system under appropriate parameters and it provides us an opportunity to make comparison between the atomic spin chain and Heisenberg spin chain.

3.1.3 Long-range case with the MDDI

To study the effects of the long-range spin coupling on the nonlinear spin wave dynamics, we need consider the spin coupling at all sites through the whole optical lattice, though the MDDI decreases rapidly in some cases. We firstly use Eq. (22) to rewrite the nonlinear motion equation of ϕ_n as

$$\begin{aligned} i\frac{d\phi_n}{dt} &= \left[\gamma_B B_z + \sum_{j\neq n} 2SJ_{nj}^{mag}\right]\phi_n - \sum_{j\neq n} SJ_{nj}^{z}\left|\phi_j\right|^2\phi_n \\ &\quad - \sum_{j\neq n} 4SJ_{nj}\phi_j(-1)^{j-n} + \sum_{j\neq n} 2SJ_{nj}|\phi_n|^2\phi_j(-1)^{j-n}. \end{aligned} \tag{38}$$

Then we set:

$$\phi_n \to \phi(y,t), \tag{39}$$

$$J_{nj}^{mag} \to J^{mag}(y-y'), \tag{40}$$

$$J_{nj} \to J(y-y'), \tag{41}$$

$$\gamma_B B_z + \sum_{j \neq n} 2SJ_{nj}^{mag} \rightarrow \omega(y). \tag{42}$$

Considering the discreteness of the optical lattice, we can treat the symbolic terms as below:

$$(-1)^{j-n} = \cos[(j-n)\pi] = \cos\left[\frac{2\pi}{\lambda_L}(y-y')\right]. \tag{43}$$

After changing the sum to integration, Eq. (38) becomes:

$$\begin{aligned} i\frac{d\phi(y,t)}{dt} = \omega(y)\phi(y,t) - \frac{2S}{\lambda_L}\phi(y,t)\int_{-\infty}^{\infty} J^{mag}(y-y')\phi^2(y',t)dy' \\ - \frac{8S}{\lambda_L}\int_{-\infty}^{\infty} J(y-y')\phi(y',t)\cos\left[\frac{2\pi}{\lambda_L}(y-y')\right]dy' \\ + \frac{4S}{\lambda_L}\phi^2(y,t)\int_{-\infty}^{\infty} J(y-y')\phi(y',t)\cos\left[\frac{2\pi}{\lambda_L}(y-y')\right]dy'. \end{aligned} \tag{44}$$

Denoting $y - y' = \xi$, the $\phi(y',t)$ can be expanded as:

$$\phi(y',t) = \phi(y,t) + \frac{\partial\phi(y,t)}{\partial y}\xi + \frac{1}{2!}\frac{\partial^2\phi(y,t)}{\partial y^2}\xi^2 + ... \tag{45}$$

Taking above series into Eq. (44), the integration variable is changed, i.e., $dy' \rightarrow -d\xi$, and using the assumption $\partial\phi(y,t)/\partial y \ll 1$, finally we get [10]:

$$\begin{aligned} i\frac{d\phi(y,t)}{dt} = -2\beta_1\frac{\partial^2\phi(y,t)}{\partial y^2} + [\omega(y) - 4\beta_0]\phi(y,t) \\ + (2\beta_0 - \gamma)|\phi(y,t)|^2\phi(y,t), \end{aligned} \tag{46}$$

where we have used $J_{ij} = \frac{1}{2}J_{ij}^{mag}$, and the coefficients are defined as below:

$$\beta_n = \frac{S}{\lambda_L}\int_{-\infty}^{\infty} J^{mag}(\xi)\xi^{2n}\cos\left(\frac{2\pi}{\lambda_L}\xi\right)d\xi, n = 0, 1, \tag{47}$$

$$\gamma = \frac{2S}{\lambda_L}\int_{-\infty}^{\infty} J^{mag}(\xi)d\xi. \tag{48}$$

The condition for Eq. (46) to have envelope soliton solution is

$$f(W) = -2\beta_1(2\beta_0 - \gamma) > 0. \tag{49}$$

From the definitions of β_n and γ, we can easily get $2\beta_0 < \gamma$. Then Eq. (49) reduces to $\beta_1 > 0$, i.e.,

$$\int J^{mag}(\xi)\xi^2\cos\left(\frac{2\pi}{\lambda_L}\xi\right)d\xi > 0. \tag{50}$$

This result is consistent with the instability condition of modulational instability of nonlinear coherent spin wave modes near the Brillouin zone boundary under the long-wavelength modulation [4]. There, the modulational instability criteria take the corresponding discrete form:

$$1 - 4A_2 + 9A_3 - 16A_4 + ... < 0, \tag{51}$$

where $A_j = J_{0j}^{mag}/J_{01}^{mag}$ ($j = 2, 3...$) is the relative strength of the longitudinal spin coupling of site j to that of NN.

The function $f(W)$ versus the transverse width W of the condensate is plotted in **Figure 3** for three different approximations. $f(W) = 0$ marked in dashed line in **Figure 3** characterize critical value, above which the magnetic solitons can occur. It is clear that the NN approximation and the NNN approximation take effect for a small transverse width.

3.2 Magnetic soliton under the LDDI

When we choose red-detuned optical lattice or an external modulational laser field is imposed into the system, both the static MDDI and the laser-induced LDDI begin to take effect on the dynamics of the soliton excitation, and the criterion for the existence of solitons could be changed. Here we also consider three interaction distances as doing in Section 3.1.

3.2.1 Nearest-neighbor approximation with the LDDI

In this case, we can obtain the continuum limit NLSE for $\phi(y,t)$ with the form:

$$i\frac{d\phi(y,t)}{dt} = 4SJ_{01}a^2\frac{d^2\phi(y,t)}{dy^2} + \left(\gamma_B B_z + 4SJ_{01}^{mag} + 8SJ_{01}\right)\phi(y,t) - 2S\left(J_{01}^{mag} + 2J_{01}\right)|\phi(y,t)|^2\phi(y,t). \tag{52}$$

The existence condition of magnetic soliton now has the form

$$f(W) = -8S^2a^2J_{01}\left(J_{01}^{mag} + 2J_{01}\right) > 0. \tag{53}$$

Obviously, magnetic soliton can be observed in this case, which is different from the case where only the MDDI plays role.

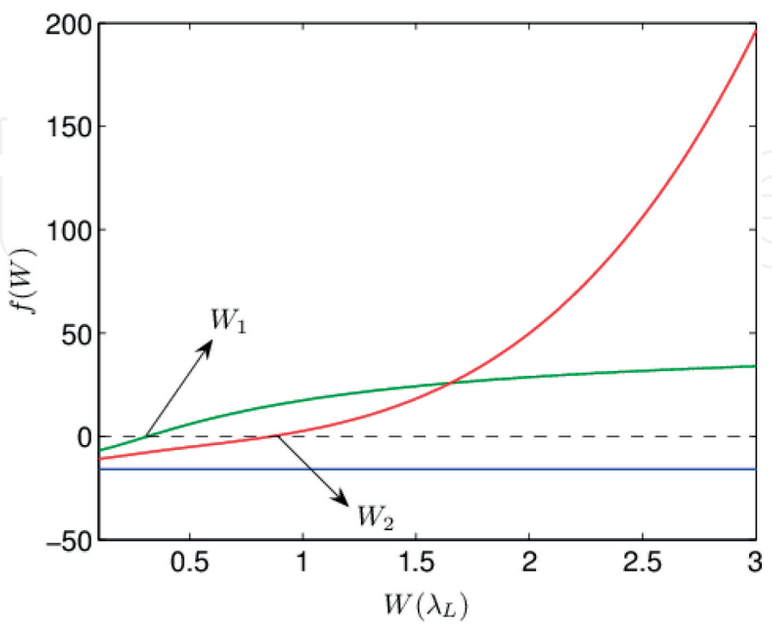

Figure 3.
The existence conditions for magnetic solitons in atomic spin chain dominated by the MDDI. The three lines correspond to the NN approximation (blue), the NNN approximation (green), and the long-range case, respectively. The critical value of the transverse width is W_1 and W_2 [10].

3.2.2 Next-nearest-neighbor approximation with the LDDI

In this case, the NLSE for $\phi(y,t)$ has the form:

$$i\frac{d\phi(y,t)}{dt} = 4SJ_{01}(1-4A_2)\frac{d^2\phi(y,t)}{dy^2}a^2 + \eta\phi(y,t) - 4SJ_{01}(1-4A_2)|\phi(y,t)|^2\phi(y,t). \tag{54}$$

We assume that the intensity of the external laser is strong enough which corresponds to strong LDDI; then the terms like J_{0j}^{mag}/J_{0j} have been ignored. So for two adjacent sites, $A_2 = J_{02}/J_{01}$ measures the relative strength of the NNN spin coupling to the NN spin coupling. The condition for Eq. (54) to have one soliton solution is

$$f(W) = -16S^2J_{01}^2(1-4A_2)(1-A_2) > 0. \tag{55}$$

3.2.3 Long-range case with the LDDI

In fact, once the external laser is imposed into the lattice, the LDDI dominates the system rapidly; the NLSE now takes the form [10]:

$$i\frac{d\phi(y,t)}{dt} = -2\beta_1\frac{\partial^2\phi(y,t)}{\partial y^2} + [\omega(y) - 4\beta_0]\phi(y,t) + (2\beta_0 - \gamma)|\phi(y,t)|^2\phi(y,t), \tag{56}$$

where the coefficients are defined as below:

$$\beta_n = \frac{2S}{\lambda_L}\int_{-\infty}^{\infty} J(\xi)\xi^{2n}\cos\left(\frac{2\pi}{\lambda_L}\xi\right)d\xi, n = 0, 1, \tag{57}$$

$$\gamma = \frac{2S}{\lambda_L}\int_{-\infty}^{\infty} J^{mag}(\xi)d\xi. \tag{58}$$

The value of β_n depends on both the MDDI and the LDDI. When a strong enough external modulated laser is imposed into the system, we have $J^{mag}(\xi) \ll J(\xi)$, which corresponds to $\gamma \ll 2\beta_0$. Thus the existence criteria of one soliton solution of Eq. (56) becomes $\beta_1\beta_0 < 0$, namely

$$f(W) = \int J(\xi)\xi^2\cos\left(\frac{2\pi}{\lambda_L}\xi\right)d\xi\int J(\xi)\cos\left(\frac{2\pi}{\lambda_L}\xi\right)d\xi < 0 \tag{59}$$

Similarly, Eq. (59) is consistent with the corresponding discrete form of MI condition of NCSW modes near the Brillouin zone boundary under the long-wavelength modulation [4]:

$$(1 - 4A_2 + 9A_3 - 16A_4 + ...)(1 - A_2 + A_3 - A_4 + ...) < 0, \tag{60}$$

where $A_j = J_{0j}/J_{01}$ ($j = 2, 3...$) is the relative strength of the transverse spin coupling of site j to that of NN.

We plot the existence regions of magnetic solitons in atomic spin chain dominated by the LDDI in **Figure 4**. The longitudinal coordinates stand for the intensity of the modulated laser. It is clear that the magnetic soliton can be achieved by

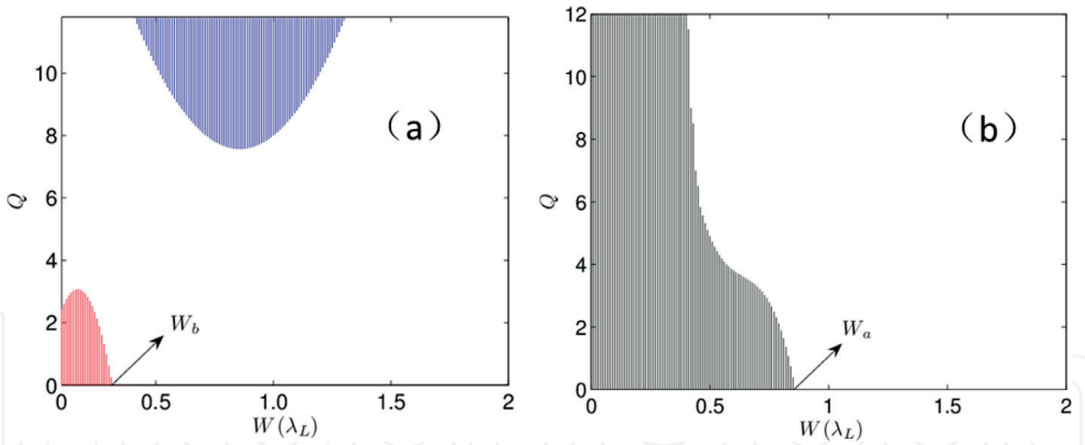

Figure 4.
The existence regions of magnetic solitons under the NNN approximation (a) and the long-range case (b) in atomic spin chain dominated by the LDDI, respectively. The critical value of the transverse width is W_a and W_b. The blank regions correspond to the existence of solitons for both cases [10].

tuning the transverse width and the modulated laser, which demonstrates the high controllability of optical lattice.

4. Conclusion

In this chapter, we have shown the existence conditions of magnetic solitons that can occur in optical lattice. Compared to the more conventional solid-state magnetic materials, we discuss how the NN, the NNN, and the long-range interactions (the MDDI and LDDI) dominate the system. We also show that they can be tuned by the laser parameters and the shape of the condensate including the laser detuning, the laser intensity, and the transverse width of the condensate.

Besides studying the magnetic solitons, the atomic spin chain in optical lattice provides us with a useful tool to study the fundamental static and dynamic aspects of magnetism and lattice dynamics [12–14]. In experimental applications, the atomic spin chain has become potential candidates for multi-bit quantum computation due to their long coherence and controllability [13, 15–17]. The theoretical study of magnetic solitons in optical lattices will play a guiding role when the optical lattice is used in cold atomic physics, condensed matter physics, and quantum information.

Acknowledgements

This work is supported by the National Natural Science Foundation of China under Grant No. 11604086. Thanks to Ying-Ying Zhang for her contributions to physics discussion and English writing of the chapter.

IntechOpen

Author details

Xing-Dong Zhao
College of Physics and Materials Science, Henan Normal University, Xinxiang, Henan, China

*Address all correspondence to: phyzhxd@gmail.com

References

[1] Li Z-D, Li L, Liu WM, Liang J-Q, Ziman T. Exact soliton solution and inelastic two-soliton collision in a spin chain driven by a time-dependent magnetic field. Physical Review E. 2003; **68**:036102

[2] Xie Z-W, Zhang W, Chui ST, Liu WM. Magnetic solitons of spinor Bose-Einstein condensates in an optical lattice. Physical Review A. 2004;**69**: 053609

[3] Kjems JK, Steiner M. Evidence for soliton modes in the one-dimensional ferromagnet $CsNiF_3$. Physical Review Letters. 1978;**41**:1137

[4] Zhao X-D, Xie ZW, Zhang W. Modulational instability of nonlinear spin waves in an atomic chain of spinor Bose-Einstein condensates. Physical Review B. 2007;**76**:214408

[5] Zhang W, Pu H, Search C, Meystre P. Spin waves in a Bose-Einstei-condensed atomic spin chain. Physical Review Letters. 2002;**88**:6

[6] Pu H, Zhang W, Meystre P. Ferromagnetism in a lattice of Bose-Einstein condensates. Physical Review Letters. 2001;**87**:140405

[7] Zhao X-D, Zhao X, Jing H, Zhou L, Zhang W. Squeezed magnons in an optical lattice: Application to simulation of the dynamical Casimir effect at finite temperature. Physical Review A. 2013; **87**:053627

[8] Zhang W, Walls DF. Gravitational and collective effects in an output coupler for a Bose-Einstein condensate in an atomic trap. Physical Review A. 1998;**57**:1248

[9] Ho TL. Spinor Bose condensates in optical traps. Physical Review Letters. 1998;**81**:742

[10] Zhao X-D, Geng Z, Zhao X, Qian J, Zhou L, Li Y, et al. Controllable magnetic solitons excitations in an atomic chain of spinor Bose-Einstein condensates confined in an optical lattice. Applied Physics B: Lasers and Optics. 2014;**115**:451-460

[11] Zobay O, Pőting S, Meystre P, Wright EM, Wright EM. Creation of gap solitons in Bose-Einstein condensates. Physical Review Letters A. 1999;**59**:643

[12] Zhao X-D, Xie Z-W, Zhang W. Nonlinear spin wave s in a Bose condensed atomic chain. Acta Physica Sinica. 2007;**56**:6358

[13] Morsch O, Oberthaler M. Dynamics of Bose-Einstein condensates in optical lattices. Reviews of Modern Physics. 2006;**78**:179

[14] Zhao X-D, Zhang Y-Y, Liu W-M. Magnetic excitation of ultra-cold atoms trapped in optical lattice. Acta Physica Sinica. 2019;**68**:043703

[15] Sundar B, Mueller EJ. Universal quantum computation with Majorana fermion edge modes through microwave spectroscopy of quasi-one-dimensional cold gases in optical lattices. Physical Review A. 2013;**88**: 063632

[16] Brennen GK, Miyake A. Measurement-based quantum computer in the gapped ground state of a two-body Hamiltonian. Physical Review Letters. 2008;**101**:010502

[17] Wasak T, Chwedeńczuk J. Bell inequality, Einstein-Podolsky-Rosen steering, and quantum metrology with spinor Bose-Einstein condensates. Physical Review Letters. 2018;**120**: 140406